

Spectroscopic characterization and molecular docking studies of acetyl ferrocene-derived Schiff base ligand with phenanthroline and some transition metal ions

W. H. Mahmoud¹ · N. F. Mahmoud¹ · G. G. Mohamed^{1,2}

Received: 18 June 2017 / Accepted: 23 September 2017
© Akadémiai Kiadó, Budapest, Hungary 2017

Abstract As a part of systematic investigation of the reactivity of a novel ferrocene-based Schiff base ligand, HL ligand was synthesized by condensation of 2-acetylferrocene with 2-aminophenol and mixed with 1,10-phenanthroline to give new mixed chelates. Series of transition metal ions Cr(III), Mn(II), Fe(III), Co(II), Ni(II), Cu(II), Zn(II) and Cd(II) complexes were synthesized. The structures of the ligand and mixed ligand complexes were confirmed by elemental analysis, spectroscopic studies [IR, ¹H NMR, UV–Vis, mass spectrometry, SEM] and thermal analysis (TG/DTG). The molar conductance measurements of the complexes in DMF determine electrolytic and non-electronic nature of the complexes. Significant applications have been done to ensure the biological importance of the new mixed metal complexes like antimicrobial activities (four bacterial organisms and four fungal organisms), anticancer activities (MCF7 breast cancer cell line) and Molecular Operating Environment studies with the crystal structure of acetylcholinesterase (PDB: 1B41), the synthetic DNA dodecamer (PDB: 1BNA) and virus protein U (Vpu) of human immune deficiency virus (HIV-1) (PDB: 2N28).

Keywords Mixed ligand chelates · IR · Molar conductance · Antimicrobial · Breast cancer · Molecular Operating Environment

Introduction

Interest in coordination chemistry is increasing continuously with the preparation of inorganic ligands containing a variety of donor groups, and it is multiplied manifold when the ligands have biological importance [1]. Schiff base complexes of transition metals are of particular interest to inorganic chemists because their structural, spectral and chemical properties are often strongly dependent on the nature of the ligand structure [2]. A large number of Schiff bases and their complexes have been studied for their interesting and important properties, e.g., their ability to reversibly bind oxygen, catalytic activity in hydrogenation of olefins, transfer of an amino group, photochromic properties and complexing ability toward some toxic metals [3]. Schiff bases are also superior reagents in biological, pharmacological, clinical and analytical applications [4]. Metal complexes of these ligands possess a wide spectrum of medicinal properties. Schiff bases and their metal complexes have played important roles in the development of chemical industries through catalysis, substrate carriers and dyes [5–7]. These ligands are widely studied because of their pronounced coordinating properties and stability [8, 9]. A number of symmetrical Schiff bases and chelates have been reported [10–13], while comparatively little is known on synthesis and physicochemical properties of Schiff base ligands and metal complexes [14–19].

So, the aim of this work is to synthesize and characterize Schiff base HL ligand (Fig. 1) and its mixed ligand chelates with 1,10-phenanthroline with eight transition metal ions: Cr(III), Mn(II), Fe(III), Co(II), Ni(II), Cu(II), Zn(II) and Cd(II), in order to study the effect of the mixed ligand systems on physicochemical properties and their biological applications.

✉ G. G. Mohamed
ggenidy@hotmail.com

¹ Chemistry Department, Faculty of Science, Cairo University, Giza 12613, Egypt

² Egypt Nanotechnology Center, Cairo University, El-Sheikh Zayed, 6th October City, Giza 12588, Egypt

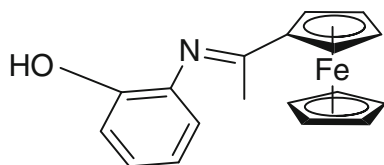


Fig. 1 Structure of ferrocene Schiff base ligand (HL)

Experimental

Material and reagent

All chemicals used were of the analytical reagent grade (AR) and of highest purity available. The chemicals used included 2-acetylferrocene which was supplied from Strem Chemicals Inc., $\text{CrCl}_3 \cdot 6\text{H}_2\text{O}$ and $\text{MnCl}_2 \cdot 2\text{H}_2\text{O}$ (Sigma-Aldrich), $\text{NiCl}_2 \cdot 6\text{H}_2\text{O}$, $\text{CoCl}_2 \cdot 6\text{H}_2\text{O}$, $\text{CuCl}_2 \cdot 2\text{H}_2\text{O}$ and $\text{ZnCl}_2 \cdot 2\text{H}_2\text{O}$ (BDH), $\text{FeCl}_3 \cdot 6\text{H}_2\text{O}$ (Prolabo), $\text{CdCl}_2 \cdot 2\text{H}_2\text{O}$ (Merck), 1,10-phenanthroline and 2-aminophenol (Merck). Organic solvents were spectroscopic pure from BDH-included ethanol, diethylether and dimethylformamide. Hydrogen peroxide, sodium chloride, sodium carbonate and sodium hydroxide (A.R.) were used. Human tumor cell line (Breast cell) was obtained frozen in liquid nitrogen ($-180\text{ }^\circ\text{C}$) from the American Type Culture Collection. The tumor cell line (MCF7) was maintained in the National Cancer Institute, Cairo, Egypt, by serial subculturing.

Solutions

A fresh stock solution of 1×10^{-3} M of 2-acetylferrocene (2 g L^{-1}) was prepared in the appropriate volume of absolute ethanol. Solutions of the Schiff base ligand and its metal complexes (1×10^{-5} M) were prepared by dilution of the previous prepared stock solutions for measuring their UV-Vis spectra.

Solution of anticancer study

A fresh stock solution of 1×10^{-3} M of Schiff base ligand (0.0016 g L^{-1}) was prepared in the appropriate volume of ethanol (95%; Sigma Chemical Co., St. Louis, Mo, USA): It was used in cryopreservation of cells. RPMI-1640 medium (Sigma Chemical Co., St. Louis, Mo, USA) was used. The medium was used for culturing and maintenance of the human tumor cell lines. The medium was supplied in a powder form. It was prepared as follows: 10.4 g medium was weighed, mixed with 2 g sodium bicarbonate, completed to 1 L with distilled water and shook carefully till complete dissolution. The medium was then sterilized by filtration in a Millipore bacterial filter ($0.22\text{ }\mu\text{m}$). The prepared medium was kept in a refrigerator ($4\text{ }^\circ\text{C}$) and

checked at regular intervals for contamination. Before use, the medium was warmed at $37\text{ }^\circ\text{C}$ in a water bath and supplemented with penicillin/streptomycin and FBS.

Sodium bicarbonate (Sigma Chemical Co., St. Louis, Mo, USA) was used for the preparation of RPMI-1640 medium. 0.05% Isotonic trypan blue solution (Sigma Chemical Co., St. Louis, Mo, USA) was prepared in normal saline and was used for viability counting. 10% Fetal bovine serum (FBS) (heat inactivated at $56\text{ }^\circ\text{C}$ for 30 min), 100 units mL^{-1} penicillin and 2 mg mL^{-1} streptomycin were supplied from Sigma Chemical Co., St. Louis, Mo, USA, and were used for the supplementation of RPMI-1640 medium prior to use. 0.025% (w/v) trypsin (Sigma Chemical Co., St. Louis, Mo, USA) was used for the harvesting of cells. 1% (v/v) Acetic acid (Sigma Chemical Co., St. Louis, Mo, USA) was used for dissolving the unbound SRB dye. 0.4% Sulforhodamine-B (SRB) (Sigma Chemical Co., St. Louis, Mo, USA) dissolved in 1% acetic acid was used as a protein dye. A stock solution of trichloroacetic acid (TCA, 50%, Sigma Chemical Co., St. Louis, Mo, USA) was prepared and stored. 50 μL of the stock was added to 200 μL RPMI-1640 medium/well to yield a final concentration of 10% used for protein precipitation. 100% Isopropanol and 70% ethanol were used. Tris base 10 mM (pH 10.5) was used for SRB dye solubilization. 121.1 g of Tris base was dissolved in 1000 mL of distilled water, and pH was adjusted by HCl acid (2 M).

Measurements

Microanalyses of carbon, hydrogen and nitrogen were carried out at the Microanalytical Center, Cairo University, Egypt, using CHNS-932 (LECO) Vario Elemental Analyzer. Analyses of the metals followed the dissolution of the solid complex in concentrated HNO_3 , neutralizing the diluted aqueous solutions with ammonia and titrating the metal solutions with EDTA. FT-IR spectra were recorded on a PerkinElmer 1650 spectrometer ($4000\text{--}400\text{ cm}^{-1}$) in KBr disks. Electronic spectra were recorded at room temperature on a Shimadzu 3101pc spectrophotometer as solutions in DMF. ^1H NMR spectra, as a solution in DMSO-d_6 , were recorded on a 300-MHz Varian-Oxford Mercury at room temperature using TMS as an internal standard. A saturated solution of the metal compound which consisted of approximately 3 mg of compound dissolved in 1 mL of D_2O was made in an NMR tube. NMR studies that included $37\text{ }^\circ\text{C}$ incubation were done in the following fashion. The initial NMR of a $37\text{ }^\circ\text{C}$ incubation study was done at room temperature before the tube was placed in the incubator at $37\text{ }^\circ\text{C}$. The NMR tube was then incubated for 20 min before it was removed from the oven and analyzed. There was about 15 min of time at room temperature to slow down the reaction for monitoring

during analysis. The NMR tube was then returned to the oven for additional incubation. The times on the 37 °C NMR studies actually refer to the total amount of time the tube was incubated in the oven. For example, a 40-min incubated sample would actually take about 70 min real time.

Molar conductivities of 10^{-3} M solutions of the solid complexes in DMF solvent were measured using Jenway 4010 conductivity meter. The thermogravimetric analyses (TG and DTG) of the solid complexes were carried out from room temperature to 1000 °C using a Shimadzu TG-50H thermal analyzer. The anticancer activity was performed at the National Cancer Institute, Cancer Biology Department, Pharmacology Department, Cairo University. The optical density (O.D.) of each well was measured spectrophotometrically at 564 nm with an ELIZA microplate reader (Meter tech. Σ 960, USA). The molecular structure of the investigated ligand was optimized by DFT-based B3LYP method along with the LANL2DZ basis set. The molecule was built with the PerkinElmer ChemBio Draw and optimized using PerkinElmer ChemBio3D software [20, 21]. The scanning electron microscopic (SEM) image of the complexes was recorded by a (Quanta FEG250) SEM, National Research Center, Egypt.

Synthesis of ferrocene Schiff base ligand HL

The new ferrocene Schiff base ligand was prepared by mixing 30 mL of hot saturated ethanolic solution of the 2-acetylferrocene (10 g, mmol) and 30 mL of hot ethanolic solution of 2-aminophenol (4.79 g, mmol). The mixture was refluxed for 3 h, and the resulting ligand was filtered and washed several times with hot ethanol until the filtrates become clear. The solid ligand then dried in desiccator over anhydrous calcium chloride. The yield was 85%.

Synthesis of metal complexes

The transition metal complexes were prepared by mixing equal amounts (0.00125 mol) of hot saturated DMF solution of the HL Schiff base ligand and 1,10-phenanthroline, with the same ratio of metal chloride (1 M:1HL:1Phen molar ratio). The mixture was refluxed for 3 h. The resulting complexes were filtered and washed several times with hot ethanol until the filtrates become clear. The solid complexes then dried in desiccator over anhydrous calcium chloride. The yield ranged from 69 to 95%.

Spectrophotometric studies

The absorption spectra of HL ligand and its metal complexes under study were scanned within the wavelength range from 200 to 700 nm.

Antimicrobial activity

The in vitro antibacterial and antifungal activity tests were performed through the well diffusion method [22] using ampicillin as positive control for Gram (+) bacteria, gentamicin for Gram (−) bacteria and amphotericin for the four fungi, respectively. The bacterial organisms used are Gram (+) bacteria: *Streptococcus pneumoniae* and *Bacillus subtilis*, Gram (−) bacteria: *Pseudomonas aeruginosa* and *Escherichia coli* and fungi like: *Aspergillus fumigatus*, *Syncephalastrum racemosum*, *Geotricum candidum* and *Candida albicans*. Stock solution (0.001 mol) was prepared by dissolving the compounds in DMSO. The nutrient agar medium for antibacterial was (0.5% peptone, 0.1% beef extract, 0.2% yeast extract, 0.5% NaCl and 1.5% agar-agar) prepared and then cooled to 47 °C and seeded with tested microorganisms. After solidification, 5-mm-diameter holes were punched by a sterile corkborer. The investigated compounds, i.e., ligand and their complexes, were introduced in petri dishes (only 0.1 mL) after dissolving in DMSO at 1.0×10^{-3} M. These culture plates were then incubated at 37 °C for 20 h for bacteria. The activity was determined by measuring the diameter of the inhibition zone (in mm). The plates were kept for incubation at 37 °C for 24 h, and then, the plates were examined for the formation of zone of inhibition. The diameter of the inhibition zones was measured in millimeters. Antimicrobial activities were performed in triplicate, and the average was taken as the final reading [23].

Anticancer activity

Potential cytotoxicity of the compounds was tested using the method of Skehan and Storeng [24]. Cells were plated in 96-multiwell plate (104 cells/well) for 24 h before treatment with the compounds to allow attachment of cell to the wall of the plate. Different concentrations of the compounds under investigation (0, 5, 12.5, 25, 50 and 100 $\mu\text{g mL}^{-1}$) were added to the cell monolayer, and triplicate wells were prepared for each individual dose. The monolayer cells were incubated with the compounds for 48 h at 37 °C and in 5% CO₂ atmosphere. After 48 h, cells were fixed, washed and stained with SRB stain. Excess stain was washed with acetic acid, and attached stain was recovered with Tris-EDTA buffer. The optical density (O.D.) of each well was measured spectrophotometrically at 564 nm with an ELIZA microplate reader, the mean background absorbance was automatically subtracted, and mean values of each drug concentration were calculated. The relation between surviving fraction and drug concentration is plotted to get the survival curve of breast tumor cell line for each compound.

Calculation:

The percentage of cell survival was calculated as follows (Eq. 1):

$$\text{Survival fraction} = \text{O.D. (treated cells)} / \text{O.D. (control cells)} \quad (1)$$

The IC_{50} values (the concentrations of the ferrocene Schiff base ligand or complexes required to produce 50% inhibition of cell growth). The experiment was repeated 3 times.

Molecular docking

Molecular Operating Environment (MOE) 2008 (MOE source: Chemical Computing Group Inc., Quebec, Canada, 2008) program was used in molecular docking studies. Firstly, a Gaussian contact surface around the binding site was sketched; Finally, docking studies were done to assess the binding free energy of the inhibitor inside the macromolecule. Autorotatable bonds were allowed; the best ten binding poses were directed to analyze for achieving the best score to compare the docking poses to the ligand in the co-crystallized structure [25].

In order to find out the possible binding modes of the most active compounds against the crystal structure of: acetylcholinesterase (PDB: 1B41), the synthetic DNA dodecamer (PDB: 1BNA) and virus protein U (Vpu) of human immune deficiency virus (HIV-1) (PDB: 2N28), molecular docking studies were performed using MOE 2008 software and it is a rigid molecular docking software [26]. The structure of ligand in PDB file format was created by Gaussian03 software. The crystal structure of: acetylcholinesterase (PDB: 1B41), the synthetic DNA dodecamer (PDB: 1BNA) and virus protein U (Vpu) of human immunodeficiency virus (HIV-1) (PDB: 2N28) was downloaded from the protein data bank (<http://www.rcsb.org/pdb>).

Results and discussion

Characterization of the ferrocene-based Schiff base ligand (HL)

The Schiff base HL ligand was prepared by the condensation of 2-acetylferrocene with 2-aminophenol in molar ratio of 1:1. The structure was identified by elemental analysis, infrared, UV-visible, ^1H NMR spectra, SEM and thermogravimetric analysis. From the investigation, the ligand is shown in Fig. 1. The infrared spectrum was consistent with the formation of the Schiff base ligand. The fundamental stretching mode of azomethine (C=N) was found at 1655 cm^{-1} , broad band at 3374 cm^{-1} assigned for

(OH) stretching mode of the phenolic hydroxyl group, a medium band at 1147 cm^{-1} assigned for (C–N) bending mode and a medium band at 1109 cm^{-1} assigned for (C–O) stretching.

^1H NMR spectrum of HL ligand showed that the chemical shift of the proton signal of the OH phenolic proton was found at 8.87 ppm. The protons of the phenyl signals were assigned at 6.38–6.65 ppm, and due to their interference, it was not possible to separate them. The chemical shifts of the protons of the ferrocene rings were assigned at 4.24–4.77 ppm, while the band at 3.32 ppm can be assigned to methyl protons. Electronic spectral data of the Schiff base HL ligand were recorded in DMF solution. The electronic spectra of the ligand exhibited three bands at 270, 326 and 428 nm. The first and second bands corresponded to $\pi \rightarrow \pi^*$ and $\pi-\pi^*$ transitions of the benzene ring and C=N group, respectively [27]. The third band corresponded to intermolecular charge transfer transitions [28].

Mass spectrum of HL ligand showed m/z peak at 318.65 amu corresponds to $(\text{C}_{18}\text{H}_{17}\text{FeNO})^+$. The proposed molecular formula of synthesized ligand was confirmed by comparing molecular formula weight 318 amu that was in good agreement with theoretical explanation.

The thermal analyses (TG and DTG) were used to confirm the suggested fragmentation patterns and determine the decomposition temperatures of the ligand. The TG data for HL Schiff base ligand (Fig. 2) showed two stages of decomposition. The first stage is within the temperature range of 125–240 °C, which correlated with evaluation of $\text{C}_7\text{H}_9\text{N}$ molecule with mass loss of 34.27% (calculated mass loss = 33.50%). The second decomposition stage in the temperature range of 240–505 °C corresponds to complete decomposition of the final part of ligand (C_{10}H_8) with mass loss 40.32% (calculated mass loss = 40.13%). The total mass loss amounted to 74.50% (calcd. 73.62%) leaving metal oxide (FeO) contaminated with carbon atom as a residue.

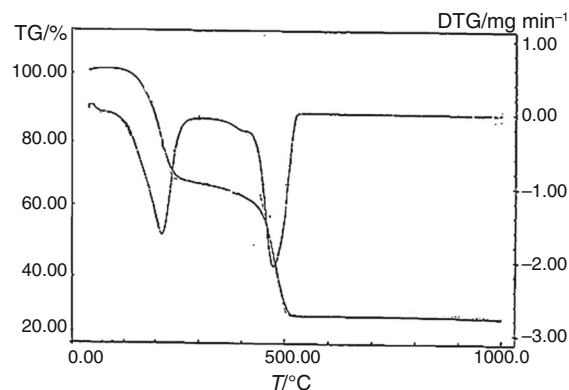


Fig. 2 TG/DTG thermal analysis of HL ligand

Characterization of the mixed ligand complexes

The Schiff base HL ligand was mixed with 1,10-phenanthroline to give eight mixed ligand chelate in the molar ratio 1:1:1 (HL–M–Phen). The isolated solid complexes were subjected to elemental analyses (C, H, N and metal content), IR, ^1H NMR, molar conductance, SEM and thermal analysis (TG/DTG) to identify their molecular structures. The IR peak shifts in (C=N) azomethine group of the complexes on comparing with that of the free ligand gave an idea about its coordination to the metal ions [29–31]. The bioefficacy of these complexes has also been screened against the growth of four bacterial species and four fungal species in vitro to evaluate their antimicrobial potential, and other biological applications have been done in order to throw more light on the effect of chelation on the ligand activity [32, 33].

Elemental analysis and molar conductivity

The elemental analyses results are summarized in Table 1. These results as well as the obtained mass spectra are in good agreement with the proposed formula. The complexes were dark brown or black in color, stable in air and soluble in different solvents like DMF and DMSO and insoluble in ethanol, methanol and water. The molar conductance values of the complexes were found to be in the range from 2.90 to 83.70 $\Omega^{-1} \text{ mol}^{-1} \text{ cm}^2$, which indicated that the

complexes were of electrolytic and non-electrolytic nature [34]. The Cr(III), Fe(III), Co(II) and Ni(II) complexes were electrolytic in nature and had molar conductivities of 83.70, 77.50, 58.10 and 57.12 $\Omega^{-1} \text{ mol}^{-1} \text{ cm}^2$, respectively. The Mn(II), Cu(II), Zn(II) and Cd(II) complexes were nonelectrolytes in nature and had molar conductivities of 21.50, 30.00, 32.20 and 2.90 $\Omega^{-1} \text{ mol}^{-1} \text{ cm}^2$, respectively. The complexes had two general formulas: one for electrolyte complexes and the other for the nonelectrolyte complexes, and they expressed as follows [35]:

Electrolytic complexes: $[\text{M}(\text{L})(\text{Phen})(\text{H}_2\text{O})_2]\text{Cl}_n$, (where $n = 2$ for $\text{M} = \text{Cr}(\text{III})$ and $\text{Fe}(\text{III})$ and $n = 1$ for $\text{M} = \text{Co}(\text{II})$ and $\text{Ni}(\text{II})$).

Non-electrolytic complexes: $[\text{M}(\text{L})(\text{Phen})(\text{Cl})(\text{H}_2\text{O})]$, ($\text{M} = \text{Mn}(\text{II}), \text{Cu}(\text{II}), \text{Zn}(\text{II})$ and $\text{Cd}(\text{II})$).

IR spectra

IR spectrum of the HL ligand exhibited a broad band at 3374 cm^{-1} for $\nu(\text{OH})$ of the phenolic group. This band shifted in the spectra of the metal complexes to 3393–3422 cm^{-1} . For $\nu(\text{C}=\text{N})$ stretching of the azomethine group, characteristic band of the Schiff base ligand in the spectrum of HL ligand appeared at 1655 cm^{-1} , but in the spectra of the mixed ligand complexes appeared in the range of 1628–1658 cm^{-1} . This was attributed to the nitrogen atom of the (C=N) group coordinated to the metal

Table 1 Analytical and physical data of HL ligand and its mixed ligand complexes with 1,10-Phen

Compound	Color	Yield %	Empirical formula (formula weight)	Elemental analysis Found (calcd%)				$\Lambda_m/\Omega^{-1} \text{ mol}^{-1} \text{ cm}^2$
				C	H	N	M	
$[\text{Cr}(\text{L})(\text{Phen})(\text{H}_2\text{O})_2]\text{Cl}_2$	Dark brown	73	$\text{C}_{30}\text{H}_{28}\text{Cl}_2\text{CrFeN}_3\text{O}_3$	54.31 (54.79)	4.20 (4.26)	6.12 (6.39)	16.10 (16.44)	83.70
$[\text{Mn}(\text{L})(\text{Phen})(\text{Cl})(\text{H}_2\text{O})]$	Dark brown	81	$\text{C}_{30}\text{H}_{26}\text{ClFeMnN}_3\text{O}_2$	59.16 (59.36)	3.99 (4.29)	6.71 (6.92)	18.04 (18.30)	21.50
$[\text{Fe}(\text{L})(\text{Phen})(\text{H}_2\text{O})_2]\text{Cl}_2$	Black	95	$\text{C}_{30}\text{H}_{28}\text{Cl}_2\text{Fe}_2\text{N}_3\text{O}_3$	56.26 (56.28)	4.06 (4.23)	5.98 (6.35)	16.40 (16.94)	77.50
$[\text{Co}(\text{L})(\text{Phen})(\text{H}_2\text{O})_2]\text{Cl}$	Black	75	$\text{C}_{30}\text{H}_{28}\text{ClCoFeN}_3\text{O}_3$	57.11 (57.28)	4.28 (4.45)	6.38 (6.68)	18.02 (18.30)	58.10
$[\text{Ni}(\text{L})(\text{Phen})(\text{H}_2\text{O})_2]\text{Cl}$	Dark brown	94	$\text{C}_{30}\text{H}_{28}\text{ClFeNiNO}_3$	56.98 (57.32)	4.19 (4.46)	6.57 (6.69)	17.83 (18.23)	57.12
$[\text{Cu}(\text{L})(\text{Phen})(\text{Cl})(\text{H}_2\text{O})]$	Black	84	$\text{C}_{30}\text{H}_{26}\text{ClCuFeN}_3\text{O}_2$	58.26 (58.54)	4.11 (4.22)	6.57 (6.83)	19.09 (19.43)	30.00
$[\text{Zn}(\text{L})(\text{Phen})(\text{Cl})(\text{H}_2\text{O})]$	Dark brown	77	$\text{C}_{30}\text{H}_{26}\text{ClFeN}_3\text{O}_2\text{Zn}$	58.16 (58.39)	3.87 (4.21)	6.56 (6.81)	19.25 (19.63)	32.20
$[\text{Cd}(\text{L})(\text{Phen})(\text{Cl})(\text{H}_2\text{O})]$	Brown	69	$\text{C}_{30}\text{H}_{26}\text{ClCdFeN}_3\text{O}_2$	54.14 (54.23)	3.83 (3.92)	6.20 (6.32)	25.11 (25.37)	2.90

ions [36–38]. A medium band appeared at 1147 cm^{-1} was assigned for (C–N) bending in the free ligand. This band was shifted to a range of $1143\text{--}1147\text{ cm}^{-1}$ in the mixed ligand complexes. Also, another medium band appeared at 1109 cm^{-1} was assigned to (C–O) stretching in the free HL ligand that shifted to a range of $1103\text{--}1108\text{ cm}^{-1}$ in the complexes. New bands appeared in the spectra of metal chelates at $948\text{--}979$ and $845\text{--}856\text{ cm}^{-1}$ could be assigned to H_2O stretching of coordinated water. Another new two bands appeared at: $563\text{--}593\text{ cm}^{-1}$ which attributed to M–O stretching and at $530\text{--}534\text{ cm}^{-1}$ which attributed to M–O stretching of coordinated water. M–N stretching bands appeared at $486\text{--}496\text{ cm}^{-1}$ [36–38]. Thus, IR data in Table 2 showed that the Schiff base ligand was coordinated to the metal ions through the two N atoms of 1,10-phenanthroline: one N atom of azomethine group and one oxygen atom of the deprotonated phenolic O of HL ligand [39].

^1H NMR spectra

The ^1H NMR spectrum of the HL Schiff base ligand displayed three significant peaks at 8.87, 6.38–6.65 and 4.24–4.77 ppm with an integration equivalent to the hydrogen protons corresponding to the (s, 1H, phenolic proton), (m, 4H, benzene ring) and (m, 9H, ferrocene rings), respectively [40, 41]. The peak at 8.87 ppm assigned for phenolic proton was disappeared in the spectra of $[\text{Zn}(\text{L})(\text{Phen})(\text{Cl})(\text{H}_2\text{O})]$ and $[\text{Cd}(\text{L})(\text{Phen})(\text{Cl})(\text{H}_2\text{O})]$ complexes, indicating that the phenolic oxygen was coordinated to the metal ions in the mixed chelates with proton displacement. The signals observed at 7.72–8.24 ppm and 7.39–7.72 ppm were assigned to aromatic ring protons of Zn(II) and Cd(II) complexes, respectively. The multiplet signals found at 6.36–6.61 ppm and 6.36–6.79 ppm were attributed to pyridine rings of Zn(II) and Cd(II) chelates, respectively. The ferrocene rings gave a group of multiplet signals at 4.23–4.78 ppm and 4.24–4.78 ppm for Zn(II) and Cd(II) complexes, respectively [42].

Mass spectral studies

The molecular ion peak of the $[\text{Ni}(\text{L})(\text{Phen})(\text{H}_2\text{O})_2]\text{Cl}$ complex was observed in its mass spectrum at 630.22 amu which confirmed the proposed formula of the complex (theoretical molecular weight 630 amu). In the mass spectrum of $[\text{Ni}(\text{L})(\text{Phen})(\text{H}_2\text{O})_2]\text{Cl}$ complex, a peak corresponding to $[\text{C}_{18}\text{H}_{17}\text{FeNO}]^+$ ion appeared as molecular ion peak at $m/z = 318.88$ amu. This peak confirmed the presence of the ferrocene Schiff base ligand in the proposed structure of the complex. However, the

Table 2 IR spectra ($4000\text{--}400\text{ cm}^{-1}$) of HL ligand and its mixed ligand complexes with 1,10-Phen

Compound assignments	HL	1,10-Phen.	$[\text{Cr}(\text{L})(\text{Phen})(\text{H}_2\text{O})_2]\text{Cl}_2$	$[\text{Mn}(\text{L})(\text{Phen})(\text{Cl})(\text{H}_2\text{O})]$	$[\text{Fe}(\text{L})(\text{Phen})(\text{H}_2\text{O})_2]\text{Cl}_2$	$[\text{Co}(\text{L})(\text{Phen})(\text{H}_2\text{O})_2]\text{Cl}$	$[\text{Ni}(\text{L})(\text{Phen})(\text{H}_2\text{O})_2]\text{Cl}$	$[\text{Cu}(\text{L})(\text{Phen})(\text{Cl})(\text{H}_2\text{O})]$	$[\text{Zn}(\text{L})(\text{Phen})(\text{Cl})(\text{H}_2\text{O})]$	$[\text{Cd}(\text{L})(\text{Phen})(\text{Cl})(\text{H}_2\text{O})]$
$\nu(\text{OH})$ stretching	3374br	–	3422br	3410br	3422br	3393br	3402br	3410br	3411br	3409br
$\nu(\text{C}=\text{N})$ stretching (Azomethene)	1655sh	1588s	1654sh	1657sh	1628m	1645sh	1652sh	1656sh	1657sh	1658sh
$\nu(\text{C}=\text{N})$ bending	1147m	–	1145s	1144m	1143m	1143m	1146m	1145m	1144m	1147s
$\nu(\text{pyridine ring})$ stretching	–	1134s	1132s	1130s	1133s	1135s	1133s	1137s	1132s	1134s
$\nu(\text{C}=\text{O})$ stretching	1109 m	–	1107m	1103sh	1105m	1105sh	1108m	1106m	1105sh	1106sh
H_2O stretching of coordinated water	–	–	962s, 845sh	969s, 848sh	979s, 856m	948s, 847sh	970s, 848sh	956s, 847sh	968s, 849sh	973s, 846sh
$\nu(\text{M}=\text{O})$ stretching	–	–	563s	583m	587s	565s	586s	586s	584s	593s
$\nu(\text{M}=\text{O})$ stretching of coordinated water	–	–	530m	532sh	531m	534m	531m	532s	532m	534m
$\nu(\text{M}=\text{N})$ stretching	–	–	489m	494sh	486m	488m	489m	496m	492m	492m

sh sharp, *m* medium, *br* broad, *s* small, *w* weak

base peak of the Ni(II) complex appeared at $m/z = 227.94$ amu. The peaks appeared at $m/z = 572.51, 402.24, 342.06, 276.01, 184.95, 108.99$ and 55.92 amu can correspond to various fragments in Ni(II) mixed ligand complex [43].

UV-Vis spectral studies

The electronic spectra of the free HL ligand and its mixed ligand complexes with 1,10-Phen were recorded in DMF solution with 10^{-5} mol L⁻¹ concentration at room temperature. Characteristic $\pi \rightarrow \pi^*$ transitions were observed in the range of 266–271 nm and 320–333 nm which attributed to transition of the benzene ring and C=N group, respectively. The bands found in the spectra of the complexes at 431–434 nm can be attributed to intermolecular charge transfer transitions. The same $\pi \rightarrow \pi^*$ transition profile was also detected for the free HL ligand at 270 nm and $\pi \rightarrow \pi^*$ transition observed at 326 nm [44].

Thermal analysis

Thermal properties of the HL ligand and its mixed ligand complexes with 1,10-Phen were investigated with TG/DTG under the ambient temperature up to 1000 °C. The thermal analysis data are summarized in Table 3. All of the

complexes gave different curves containing different decomposition steps. The experimental weight loss values for the complexes were in good agreement with the calculated values [45].

The TG curve of [Cr(L)(Phen)(H₂O)₂]Cl₂ complex showed three decomposition steps within the temperature range of 60–545 °C. The first and second decomposition steps were accompanied by loss of C₁₅H₁₇Cl₂N₂ fragment in the temperature range of 60–320 °C with an estimated mass loss of 45.64% (calcd. 45.05%). The third stage of decomposition showed loss of C₉H₁₁NO_{0.5} fragment at 320–545 °C with an estimated mass loss of 21.21% (calcd. 21.46%). Thereafter, the percentage of the residue corresponds to chromium oxide contaminated with iron(II) oxide and carbon atoms. The total estimated mass loss was found to be 66.51% (calcd. 66.84%).

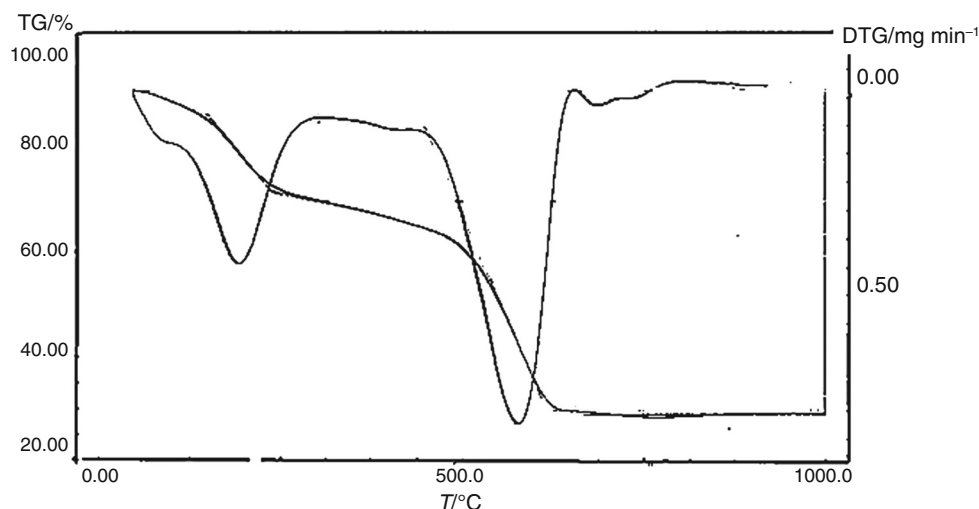
TG curve of the [Mn(L)(Phen)(Cl)(H₂O)] complex showed three steps of decomposition. The first stage of decomposition occurred in the 160–390 °C temperature range, corresponding to the loss of C₁₅H₁₇Cl₂N₂ fragment, and was accompanied by a mass loss of 38.65% (calcd. 38.99%). The second and third stages of decomposition involved the removal of C₁₂H₉N fragment in the 390–490 °C temperature range and were accompanied by mass loss of 28.17% (calcd. 27.53%). The total mass loss

Table 3 Thermoanalytical results (TG and DTG) of HL ligand and its mixed ligand complexes with 1,10-Phen

Compound	TGA range/ °C	$T_g/^\circ\text{C}$	n^*	Mass loss%		Total mass loss % Found (calcd)	Assignment	Residue
				Found	Calcd.			
HL	125–237	205	1	34.27	33.5	74.5	Loss of C ₇ H ₉ N	FeO + C
	238–504	471	1	40.32	40.13	(73.62)	Loss of C ₁₀ H ₈	
[Cr(L)(Phen)(H ₂ O) ₂]Cl ₂	60–320	109, 281	2	45.64	45.05	66.51	Loss of C ₁₅ H ₁₇ Cl ₂ N ₂	1/2 Cr ₂ O ₃ + FeO + 6C
	320–545	407, 589	1	21.21	21.46	(66.84)	Loss of C ₉ H ₁₁ NO _{0.5}	
[Mn(L)(Phen)(Cl)(H ₂ O)]	160–390	207	1	38.65	38.99	66.83	Loss of C ₁₃ H ₁₇ ClN ₂	MnO + FeO + 5C
	390–490	370, 453	2	28.17	27.53	(66.52)	Loss of C ₁₂ H ₉ N	
[Fe(L)(Phen)(H ₂ O) ₂]Cl ₂	100–530	162, 458	2	69.28	69.74	69.28 (69.74)	Loss of C ₂₆ H ₂₈ Cl ₂ N ₃ O _{0.5}	1/2 Fe ₂ O ₃ + FeO + 4C
[Co(L)(Phen)(H ₂ O) ₂]Cl	120–265	195	1	20.47	19.97	65.16	Loss of C ₃ H ₁₂ ClN ₃	CoO + FeO + 6C
	265–830	513, 655	2	44.96	45.19	(65.43)	Loss of C ₂₁ H ₁₆ O	
[Ni(L)(Phen)(H ₂ O) ₂]Cl	80–410	135, 241,	3	31.72	31.61	69.03	Loss of C ₁₀ H ₁₅ ClN ₂	NiO + FeO + 4C
	410–650	376	2	37.19	37.42	(69.63)	Loss of C ₁₆ H ₁₃ NO	
		447, 606						
[Cu(L)(Phen)(Cl)(H ₂ O)]	120–240	186	1	23.94	23.98	70.20	Loss of C ₆ H ₁₂ ClN ₂	CuO + FeO + 2C
	240–700	554, 507	2	46.27	47.47	(71.46)	Loss of C ₂₂ H ₁₄ N	
[Zn(L)(Phen)(Cl)(H ₂ O)]	150–470	195, 425	2	40.03	40.63	73.11	Loss of C ₁₄ H ₁₉ ClN ₂	ZnO + FeO + C
	470–655	604	1	33.08	32.60	(73.23)	Loss of C ₁₅ H ₇ N	
[Cd(L)(Phen)(Cl)(H ₂ O)]	156–330	197, 312	2	32.17	32.00	66.26	Loss of C ₁₁ H ₁₇ ClN ₂	CdO + FeO + 2C
	330–526	492	1	34.09	34.19	(66.19)	Loss of C ₁₇ H ₉ N	

n^* = number of decomposition steps

Fig. 3 TG/DTG thermal analysis of [Cu(L)(Phen)(Cl)(H₂O)] complex. **a** In case of Cr(III), Fe(III), Co(II) and Ni(II) complexes (where $n = 2$ for Cr(III) and Fe(III) complexes and $n = 1$ for Co(II) and Ni(II) complexes). **b** In case of Mn(II), Cu(II), Zn(II) and Cd(II) complexes



amounted to 66.83% (calcd. 66.52%), and manganese oxide contaminated with iron(II) oxide and carbon atoms was remained as a residue.

The [Fe(L)(Phen)(H₂O)₂Cl₂] complex exhibited two decomposition steps. The first and second steps occurred in the temperature range of 100–530 °C. These steps assigned to loss of C₂₆H₂₈Cl₂N₃O_{0.5} fragment with estimated mass loss of 69.28% (calcd. = 69.74%). The overall mass loss amounted to 69.28% (calcd. = 69.74%) leaving ½Fe₂O₃, FeO and contaminated carbon as the residue of decomposition.

The TG curve of [Co(L)(Phen)(H₂O)₂Cl] complex showed three decomposition steps within the temperature range of 120–830 °C. The first decomposition step was accompanied by loss of C₃H₁₂ClN₃ fragment in the temperature range of 120–265 °C with an estimated mass loss of 20.47% (calcd. 19.97%). The second and third stages of decomposition showed loss of C₂₁H₁₆O fragment at 265–830 °C with an estimated mass loss of 44.96% (calcd. 45.19%). Thereafter, the percentage of the residue corresponds to CoO and FeO oxides contaminated with carbon atoms and the total estimated mass loss was found to be 65.16% (calcd. 65.43%).

TG curve of the [Ni(L)(Phen)(H₂O)₂Cl] complex showed five steps of decomposition. The first, second and third stages of decomposition occurred in the 80–410 °C temperature range, corresponding to the loss of C₁₀H₁₅.ClN₂ fragment, and were accompanied by a mass loss of 31.72% (calcd. 31.61%). The fourth and five stages of decomposition involved the removal of C₁₆H₁₃NO fragment in the 410–650 °C temperature range and were accompanied by mass loss of 37.19% (calcd. 37.42%). The total mass loss amounted to 69.03% (calcd. 69.63%) NiO contaminated with FeO, and carbon atoms were remained as a residue.

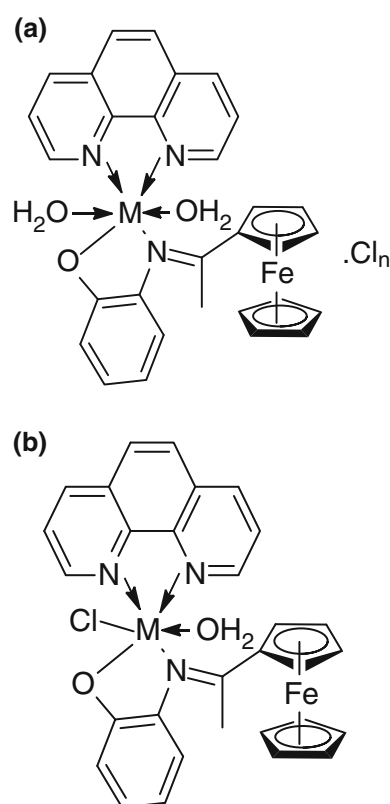
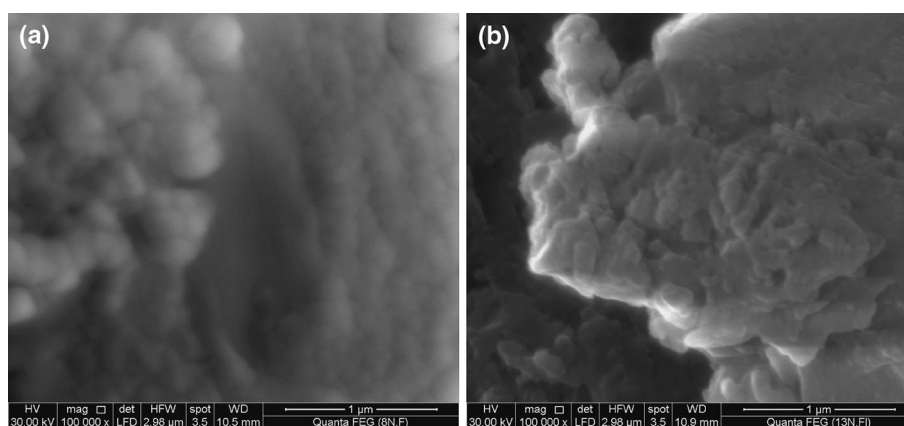


Fig. 4 Structure of HL Schiff base metal complexes

[Cu(L)(Phen)(Cl)(H₂O)] complex (Fig. 3) showed only three decomposition steps around 120–700 °C. The first decomposition step occurred at 120–240 °C with a mass loss of 23.94% (calcd. 23.98%) corresponding to the loss of C₆H₁₂ClN₂ fragment. The second and third steps of decomposition occurred at 240–700 °C with a mass loss of 46.27% (calcd. 47.47%) corresponding to the loss of C₂₂H₁₄N fragment. The total mass loss was 70.20% (calcd.

Fig. 5 SEM image of **a** HL ligand and **b** $[\text{Cr}(\text{L})(\text{Phen})(\text{H}_2\text{O})_2]\text{Cl}_2$ complex



71.46%) leaving CuO contaminated with FeO and carbon atoms as a residue.

The TG curve of $[\text{Zn}(\text{L})(\text{Phen})(\text{Cl})(\text{H}_2\text{O})]$ complex showed three decomposition steps within the temperature range of 150–655 °C. The first and second decomposition steps were accompanied by loss of $\text{C}_{14}\text{H}_{19}\text{ClN}_2$ fragment in the temperature range of 150–470 °C with an estimated mass loss of 40.03% (calcd. 40.63%). The third stage of decomposition showed loss of $\text{C}_{15}\text{H}_7\text{N}$ fragment at 470–655 °C with an estimated mass loss of 33.08% (calcd. 32.60%). Thereafter, the percentage of the residue

corresponds to zinc oxide, iron oxide and carbon atom and the total estimated mass loss was found to be 73.11% (calcd. 73.23%).

The $[\text{Cd}(\text{L})(\text{Phen})(\text{Cl})(\text{H}_2\text{O})]$ chelate exhibited three decomposition steps. The first and second steps occurred in the temperature range of 150–330 °C. These steps assigned to loss of $\text{C}_{11}\text{H}_{17}\text{ClN}_2$ fragment with an estimated mass loss of 32.17% (calcd. 32.00%). The third stage of decomposition showed loss of $\text{C}_{17}\text{H}_9\text{N}$ fragment at 330–530 °C with an estimated mass loss of 34.09% (calcd. 34.19%). The overall mass loss amounted to 66.26%

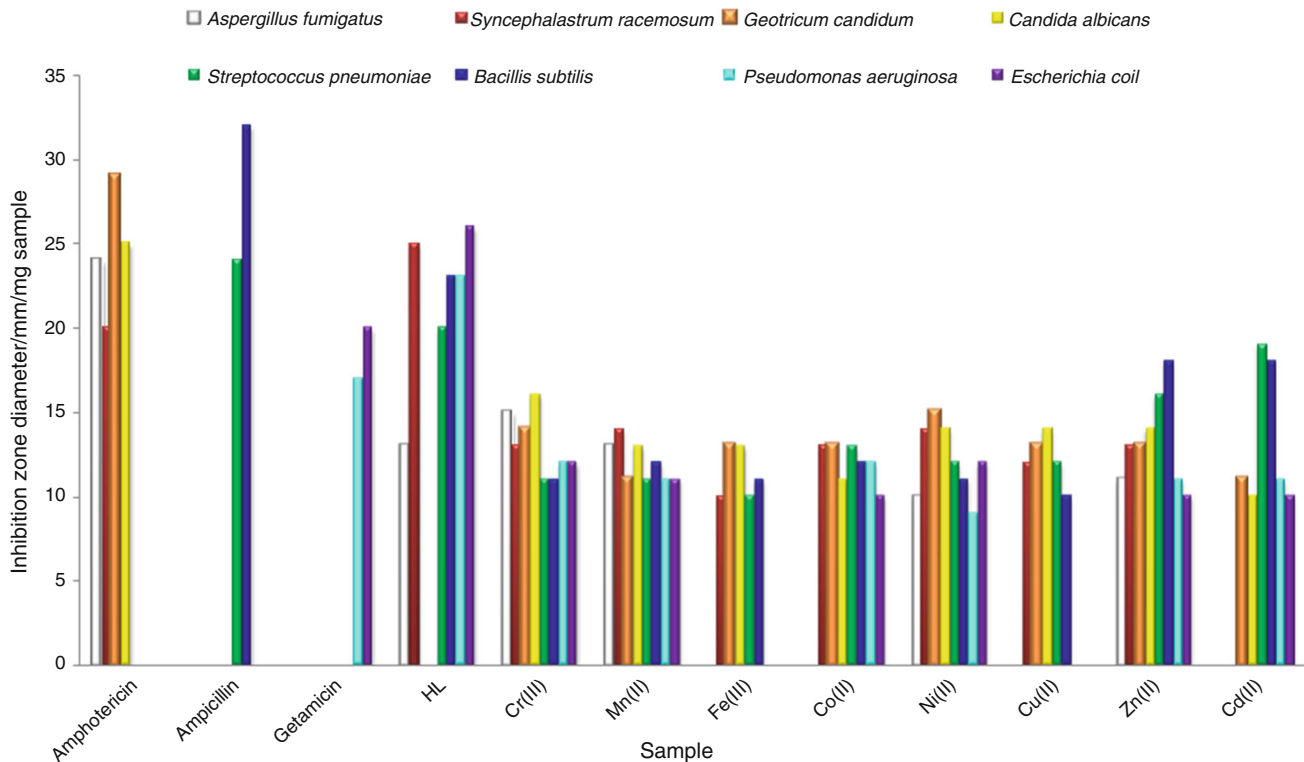


Fig. 6 Biological activity of ferrocene Schiff base ligand and its mixed ligand complexes with 1,10-Phen

Table 4 Biological activity of HL ligand and its mixed ligand complexes with 1,10-Phen

Sample	Inhibition zone diameter (mm/mg sample)									
	(Fungi)					bacteria				
	<i>Aspergillus fumigatus</i>	<i>Syncephalastrum racemosum</i>	<i>Geotricum candidum</i>	<i>Candida albicans</i>	Gram (+) bacteria	Gram (-) bacteria				
Standard (1): Amphotericin	24	20	29	25	-	-	-	-	-	-
Standard (2): Ampicillin	-	-	-	-	24	32	-	-	-	-
Standard (3): Getamicin	-	-	-	-	-	-	17	20	26	26
HL	13	25	0	0	20	23	23	12	12	12
[Cr(L)(Phen)(H ₂ O) ₂][Cl ₂]	15	13	14	16	11	11	12	11	11	11
[Mn(L)(Phen)(Cl)(H ₂ O)]	13	14	11	13	11	12	11	0	0	0
[Fe(L)(Phen)(H ₂ O) ₂][Cl ₂]	0	10	13	13	10	11	12	12	10	10
[Co(L)(Phen)(H ₂ O) ₂][Cl]	0	13	13	11	13	12	12	9	12	12
[Ni(L)(Phen)(H ₂ O) ₂][Cl]	10	14	15	14	12	11	11	10	0	0
[Cu(L)(Phen)(Cl)(H ₂ O)]	0	12	13	14	12	10	0	11	10	10
[Zn(L)(Phen)(Cl)(H ₂ O)]	11	13	13	14	16	18	11	18	10	10
[Cd(L)(Phen)(Cl)(H ₂ O)]	0	0	11	10	19	18	11	18	10	10

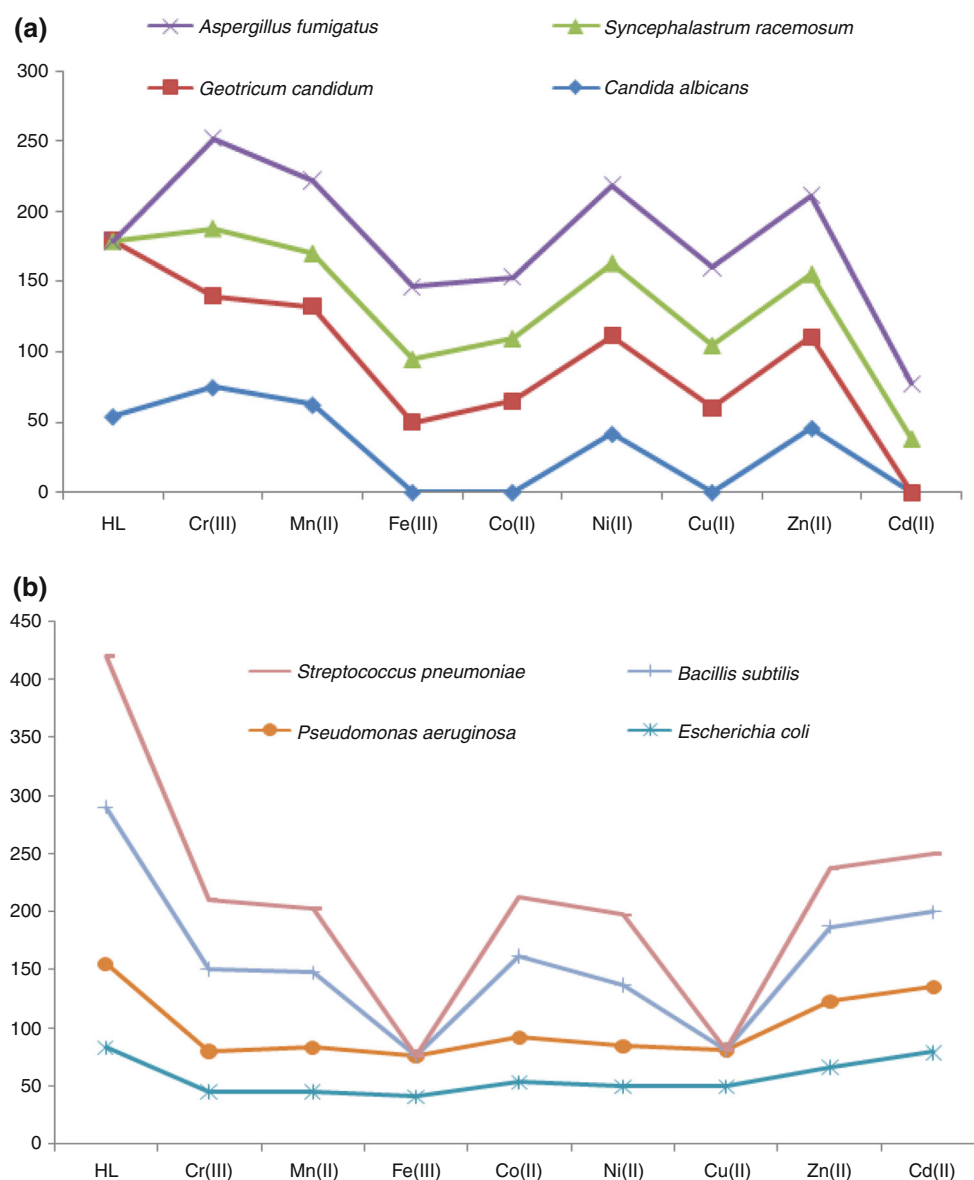


Fig. 7 Activity index of ferrocene Schiff base ligand and its mixed metal complexes with 1,10-Phen against: **a** different fungal species and **b** different bacterial species

(calcd. = 66.19%) leaving CdO, FeO and carbon as the residue of decomposition.

Structural interpretation

The structures of mixed ligand complexes of HL with 1,10-Phen and some transition metal ions: Cr(III), Mn(II), Fe(III), Co(II), Ni(II), Cu(II), Zn(II) and Cd(II) were confirmed from elemental analyses, IR, ^1H NMR, UV-visible spectra, molar conductance, SEM and thermal analyses (TG and DTG) [46–48]. The proposed structural formulae of the complexes were listed as two types of coordination as shown in Fig. 4.

SEM studies

The SEM analysis was carried out to check the surface morphology of the selected HL ligand and its Cr(III) mixed ligand complex with 1,10-Phen, and the micrographs obtained are given in Fig. 5. The micrograph of the Schiff base ligand given in Fig. 5a showed the presence of well-defined crystals free from any shadow, and its external surface had a twisted fiber and grass-like morphology. On the other hand, the micrograph of chromium(III) complex, Fig. 5b, showed a rock-like appearance with a numerous territorial patches. These facts revealed the amorphous nature of the complex with complicated interpretation due

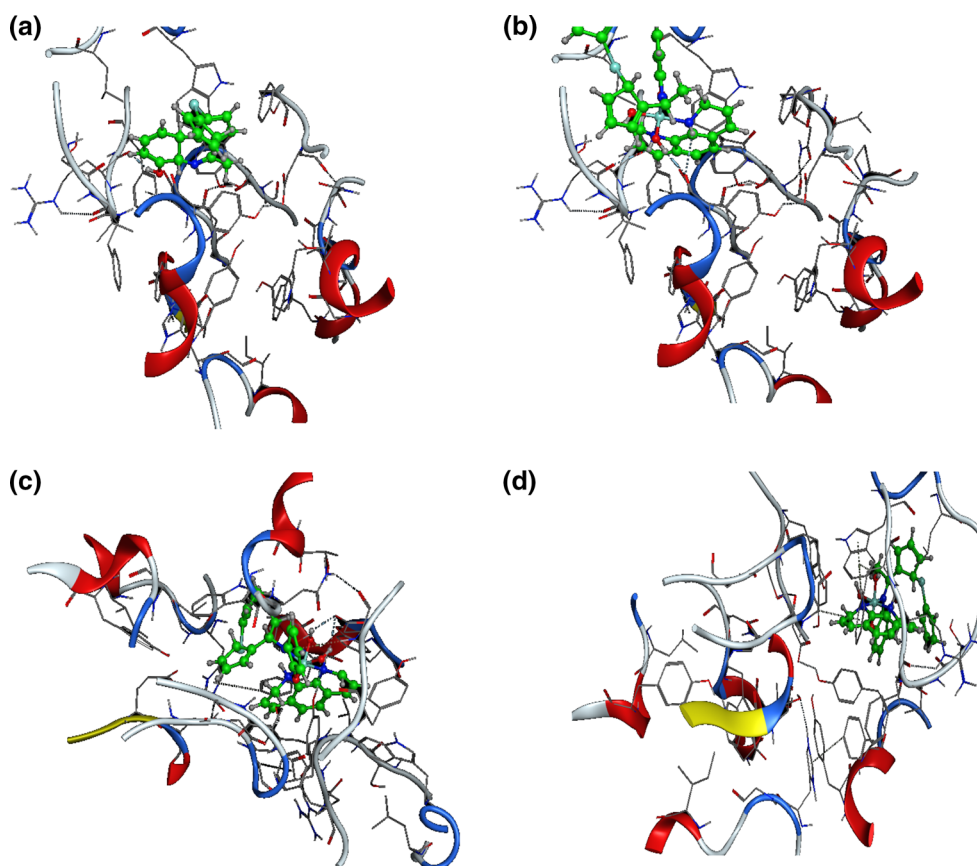


Fig. 8 3D plot of the interaction against receptors of 1B41 with: **a** ferrocene Schiff base ligand HL, **b** $[\text{Co}(\text{L})(\text{Phen})(\text{H}_2\text{O})_2]\text{Cl}$, **c** $[\text{Zn}(\text{L})(\text{Phen})(\text{Cl})(\text{H}_2\text{O})]$ and **d** $[\text{Cd}(\text{L})(\text{Phen})(\text{Cl})(\text{H}_2\text{O})]$ complexes

to unclear appearance. It was evident from the SEM study that in the synthesized metal complex, semi-crystals were found to grow up from just a single molecule to several molecules in an aggregate distribution with particle sizes of few nanometers. In addition, different characteristic shape of metal Schiff base complex was identified and this SEM image was quite different from that of HL Schiff base. The average particle size of HL ligand was 37.88 nm, but the average particle size of the $[\text{Cr}(\text{L})(\text{Phen})(\text{H}_2\text{O})_2]\text{Cl}_2$ complex was 26.39 nm [49].

Antimicrobial activity

Antibacterial activity of HL ligand and its mixed ligand complexes with 1,10-phenanthroline was tested against different bacterial species: two Gram (+) *Streptococcus pneumoniae* and *Bacillus subtilis* and two Gram (–) *Pseudomonas aeruginosa* and *Escherichia coli* by using modified agar diffusion method. Their activities were compared with standards antibiotics such as ampicillin and gentamicin. The antibacterial results displayed in Fig. 6 suggested that Cr(III), Mn(II), Fe(III), Co(II), Ni(II),

Cu(II), Zn(II) and Cd(II) metal complexes showed potential antibacterial activity. Ferrocene-based Schiff HL ligand showed antibacterial activity with inhibition zone diameters of 13.0–26.0 mm. Either Fe(III) or Cu(II) complexes showed weak activity with inhibition zone diameters of 10.0–12.0 mm. The Co(II), Zn(II) and Cd(II) complexes showed great activity with inhibition zone diameters of 10–19 mm that are summarized in Table 4. This higher antimicrobial activity of the metal complexes compared with that of Schiff base was perhaps due to the change in structure due to coordination and chelating tends to make metal complexes acted as more powerful and potent bacteriostatic agents, thus inhibiting the growth of the microorganisms [50, 51].

On the other hand, antifungal activity of Schiff base HL ligand and its mixed ligand complexes also was tested against different fungal microorganisms: *Aspergillus fumigatus*, *Syncephalastrum racemosum*, *Geotricum candidum* and *Candida albicans* by using modified agar diffusion method. The antifungal results suggested that metal complexes showed potential antifungal activity with inhibition zone diameters of 11–25 mm. According to

Table 5 Energy values obtained in docking calculations of HL and Co(II) complex with the crystal structure of: acetylcholinesterase (PDB: 1B41), the synthetic DNA dodecamer (PDB: 1BNA) and virus protein U (Vpu) of human immune deficiency virus (HIV-1) (PDB: 2N28)

Receptor	Ligand moiety	Receptor site	Interaction	Distance/Å	E/kcal mol ⁻¹
1B41	O 36	O ARG 296	H-donor	3.06	- 1.8
	C 7	6-ring TRP 286	H-Pi	4.37	- 0.6
1BNA	Fe 25	OP1 DA 18	Metal	2.16	- 2.7
	C21	OP1 DA 18	Ionic	3.84	- 0.9
	5-ring	C4' DA 17	H-Pi	4.41	- 0.6
2N28	O36	O HIS 72	H-donor	2.92	- 2.7
	C21	OE1 GLU 69	Ionic	3.06	- 4.1
	C21	OE2 GLU 69	Ionic	3.75	- 1.1
Receptor	Co-complex moiety	Receptor site	Interaction	Distance/Å	E/kcal mol ⁻¹
1B41	N39	O TYR 341	H-donor	3.50	- 0.8
	N58	O SER 293	H-donor	3.20	- 1.9
	O64	O TYR 341	H-donor	2.83	- 4.2
1BNA	N39	OP2 DT 19	H-donor	3.28	- 3.1
	N58	OP1 DT 19	H-donor	3.09	- 2.8
	O64	OP1 DT 19	H-donor	2.74	- 7.0
	Fe24	OP2 DT 20	Metal	2.33	- 2.8
	N39	OP1 DT 19	Ionic	3.38	- 2.4
	N39	OP2 DT 19	Ionic	3.28	- 2.8
	N39	OP2 DT 19	Ionic	3.28	- 2.8
2N28	N39	OE1 GLU 69	H-donor	2.88	- 16.8
	O64	OE2 GLU 69	H-donor	2.79	- 6.8
	Fe24	O HIS 72	Metal	2.54	- 0.9
	N39	OE1 GLU 69	Ionic	2.88	- 5.3
	N39	OE2 GLU 69	Ionic	3.31	- 2.7

Overtone's concept of cell permeability, the lipid membrane that surrounded the cell favored the passage of only the lipid soluble materials due to which liposolubility was an important factor, which controlled the antimicrobial activity. On chelation, the polarity of the metal ion would be reduced to a greater extent due to the overlap of the ligand orbital and partial sharing of the positive charge of the metal ion with donor groups. Further, it increased the delocalization of π -electrons over the whole chelate ring and enhanced the lipophilicity of the complexes. This increased lipophilicity enhanced the penetration of the complexes into lipid membranes and blocking of the metal binding sites in the enzymes of microorganisms. These complexes also disturbed the respiration process of the cell and thus blocked the synthesis of the proteins that restricted further growth of the organisms [52].

The activities of the prepared HL ligand and its mixed ligand complexes were confirmed by calculating the activity index according to the following relation (Eq. 2) [53, 54]:

Activity index (A)

$$= \frac{\text{Inhibition Zone of compound (mm)}}{\text{Inhibition Zone of standard drug (mm)}} \times 100 \quad (2)$$

From the data, it was concluded that Cd(II) complex had the highest activity index, while Fe(III) complex had the lowest activity index, see Fig. 7 [55].

Anticancer activity

The cytotoxic properties of the selected mixed ligand complexes and their free ferrocene-based Schiff base ligand (HL) were screened against breast cancer cell line MCF7. The pharmacological results showed that all the metal complexes were inactive against MCF7 cell line except the Mn(II) mixed ligand complex showed great cytotoxic activity. It had IC₅₀ of 4.5 $\mu\text{g mL}^{-1}$ which considered as very low concentration of the metal complex to kill 50% of the breast cancer cell line MCF7. The HL ligand showed very weak cytotoxic activity and IC₅₀ of

Table 6 Energy values obtained in docking calculations of Zn(II) and Cd(II) complexes with the crystal structure of: acetylcholinesterase (PDB: 1B41), the synthetic DNA dodecamer (PDB: 1BNA) and virus protein U (Vpu) of human immune deficiency virus (HIV-1) (PDB: 2N28)

Receptor	Zn-complex moiety	Receptor site	Interaction	Distance/Å	<i>E</i> /kcal mol ⁻¹
1B41	O64	OD2 ASP 74	H-donor	2.63	- 0.8
	O66	OD2 ASP 74	H-donor	3.03	- 0.7
	O66	OH TYR 124	H-acceptor	2.80	- 0.8
	6-ring	N ASP 74	Pi-H	4.61	- 0.9
1BNA	N39	OP1 DT 19	H-donor	2.77	- 16.6
	N64	OP1 DT 19	H-donor	2.89	- 6.0
	N39	OP1 DT 19	Ionic	2.77	- 6.2
2N28	N39	OE1 GLU 69	H-donor	2.71	- 19.1
	O64	OE1 GLU 69	H-donor	2.72	- 9.0
	N39	OE1 GLU 69	Ionic	2.71	- 6.7
	N39	OE2 GLU 69	Ionic	3.79	- 1.0
Receptor	Cd(II)-complex moiety	Receptor site	Interaction	Distance/Å	<i>E</i> /kcal mol ⁻¹
1B41	N58	5-Ring TRP 286	H-Pi	4.46	- 1.7
	N58	6-Ring TRP 286	H-Pi	3.91	- 1.9
	O64	6-Ring TRP 286	H-Pi	4.28	- 0.7
1BNA	N58	O3' DC 11	H-donor	3.35	- 1.2
	N58	OP1 DG3 12	H-donor	3.29	- 5.9
	O64	OP1 DG3 12	H-donor	2.80	- 3.8
	6-ring	C4' DA 17	Pi-H	3.82	- 0.6
2N28	N39	OE1 GLU 69	H-donor	2.71	- 19.0
	O64	OE1 GLU 69	H-donor	3.74	- 0.9
	N39	OE2 GLU 69	Ionic	2.61	- 5.4
	N39	OE2 GLU 69	Ionic	3.80	- 1.4

58.0 µg mL⁻¹ that means Mn(II) mixed ligand complex has great cytotoxic activity than HL ligand itself [56].

Molecular modeling of HL ligand: Docking Study

All docked compounds, HL ligand and Co(II), Zn(II) and Cd(II) mixed ligand complexes, were represented in balls and stick to clarify suggesting the preferred binding mode of compounds in the target crystal structure (Figs. 8–10). Also, the current ligand–receptor interactions were analyzed on the basis of energy scores as described in Tables 5 and 6 [57].

Acetylcholinesterase (AChE) is among the most efficient enzymes with a turnover number of > 104 s⁻¹. While the structural and mechanistic origin of its catalytic power and high reactivity toward organophosphorus inhibitors has been a subject of interest for several decades, only recently it has been possible to delineate the unique functional architecture of the AChE active center. Knowledge of the structural and functional properties of AChE, in particular those of human AChE (hAChE), is important for the design of anti-Alzheimer drugs [58]. Improved procedures were

developed for treatment of intoxication by nerve agents and for the design of safer and more effective insecticides by comparison with the three-dimensional structure of the insect enzyme [59, 60].

Studying the binding of HL and its mixed ligand complexes with crystal structure of acetylcholinesterase (PDB: 1B41) gave the minimum binding energy was found to be - 4.2 kcal mol⁻¹ for [Co(L)(Phen)(H₂O)₂]Cl complex. The minimum energy docked pose revealed that the Co(II) complex fitted into the curve contour of the targeted protein in the groove. Moreover, -OH group of the Co(II) complex acted as strong H-bond donors and was engaged in hydrogen-bonding interactions with oxygen atom of O TYR 341 of Tyrosine amino acid [61], see Fig. 8 and Tables 5 and 6.

The crystal structure of the synthetic DNA dodecamer (CpGpCpGpApApTpTpCpGpCpG) has been refined to a residual error of *R* = 17.8% at 1.9-Å resolution (two-σ data). The molecule forms slightly more than one complete turn of right handed double-stranded B helix. The two ends of the helix overlap and interlock minor grooves with neighboring molecules up and down a 21 screw axis,

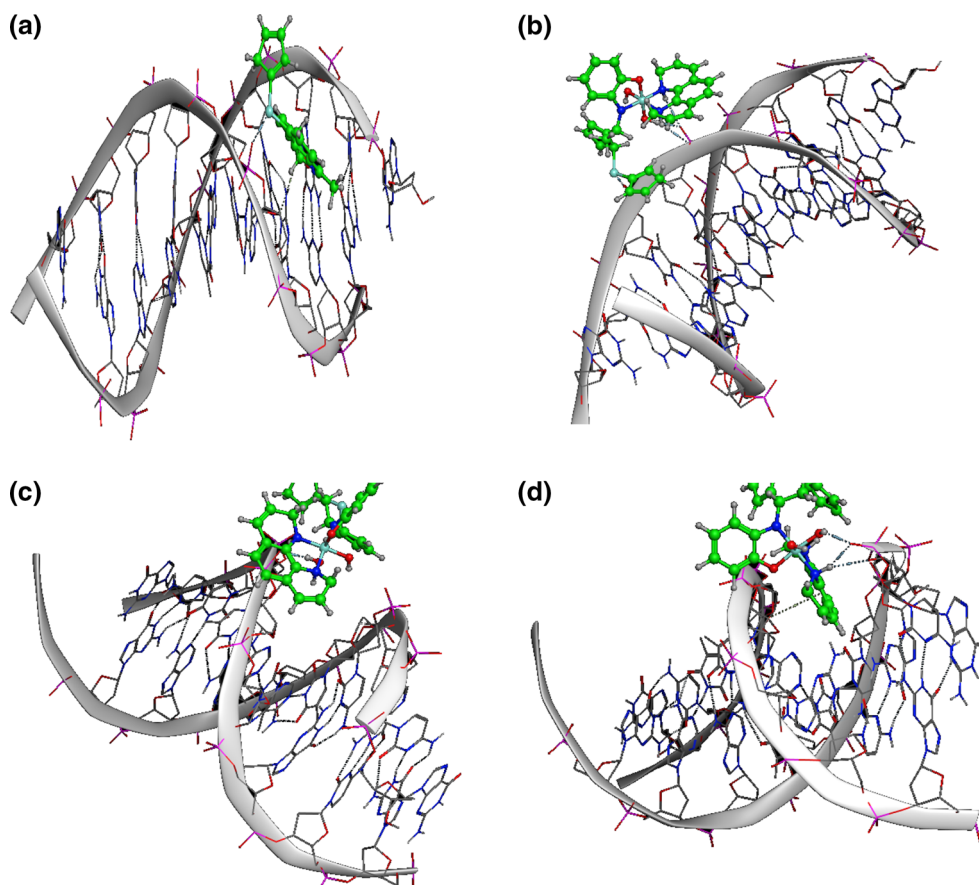
producing a 190 bend in helix axis over the 11-base-pair steps of the dodecamer [62]. From the data presented in Tables 5 and 6, the Zn(II) complex showed highest interaction with minimum binding energy of $-16.6 \text{ kcal mol}^{-1}$ with the crystal structure of the synthetic DNA dodecamer (PDB ID: 1BNA), see Fig. 9.

Virus protein U (Vpu) is one of the accessory proteins encoded by human immunodeficiency HIV-1 virus of AIDS. Although it is dispensable for viral replication in vitro, it has multiple biological functions that are crucial for viral infectivity in vivo. Vpu removes newly synthesized CD4 receptors from the endoplasmic reticulum (ER) and causes their subsequent degradation. As a result, it prevents CD4 receptors from binding to the viral envelope (Env) precursor gp160, thereby enhancing viral infectivity. Vpu also enhances the release of newly formed virus particles by antagonizing the human immune restriction factor BST-2/CD317 (tethering), which otherwise prevents their release. Recently, Vpu has been shown to induce down modulation of natural killer (NK) cell receptor NK, T cell and B cell antigen (NTB-A) from the cell surface and prevent HIV infected cells from degranulation and lysis by NK cells [63–66].

From the data summarized in Tables 5 and 6, it was found that all of the tested compounds were interacted with the protein receptors through a hydrogen bond, ionic and metal interaction. The values of interaction energies revealed that Zn(II) complex had the most stable interaction than the other complexes and free HL ligand with minimum binding energy of $-19.1 \text{ kcal mol}^{-1}$, see Fig. 10.

The histogram of the binding energy ($-E \text{ kcal mol}^{-1}$) between HL ligand and its Co(II), Zn(II) and Cd(II) mixed ligand chelates with 1,10-phenanthroline with crystal structures of: acetylcholinesterase (PDB: 1B41), the synthetic DNA dodecamer (PDB: 1BNA) and virus protein U (Vpu) of human immunodeficiency virus (HIV-1) (PDB: 2N28) is shown in Fig. 11. The histogram showed that the $[\text{Zn(L)(Phen)(Cl)(H}_2\text{O)}]$ had the minimum binding energy of -0.8 , -16.6 and $-19.1 \text{ kcal mol}^{-1}$ with the receptors of 1B41, 1BNA and 2N28, respectively.

Fig. 9 3D plot of the interaction against receptors of 1BNA with: **a** ferrocene Schiff base ligand HL, **b** $[\text{Co(L)(Phen)(H}_2\text{O)}_2]\text{Cl}$, **c** $[\text{Zn(L)(Phen)(Cl)(H}_2\text{O)}]$ and **d** $[\text{Cd(L)(Phen)(Cl)(H}_2\text{O)}]$ complexes



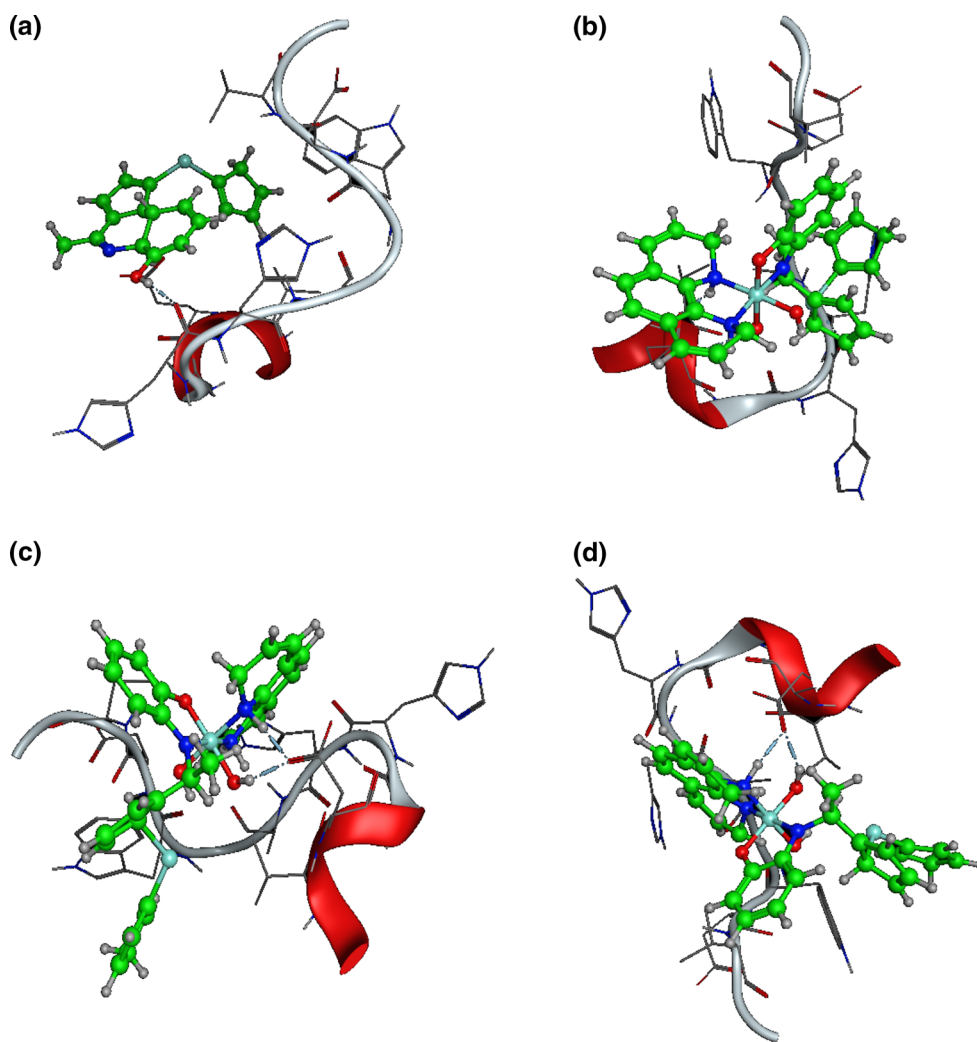


Fig. 10 3D plot of the interaction against receptors of 2N28 with: **a** ferrocene Schiff base ligand HL, **b** $[\text{Co}(\text{L})(\text{Phen})(\text{H}_2\text{O})_2]\text{Cl}$, **c** $[\text{Zn}(\text{L})(\text{Phen})(\text{Cl})(\text{H}_2\text{O})]$ and **d** $[\text{Cd}(\text{L})(\text{Phen})(\text{Cl})(\text{H}_2\text{O})]$ complexes

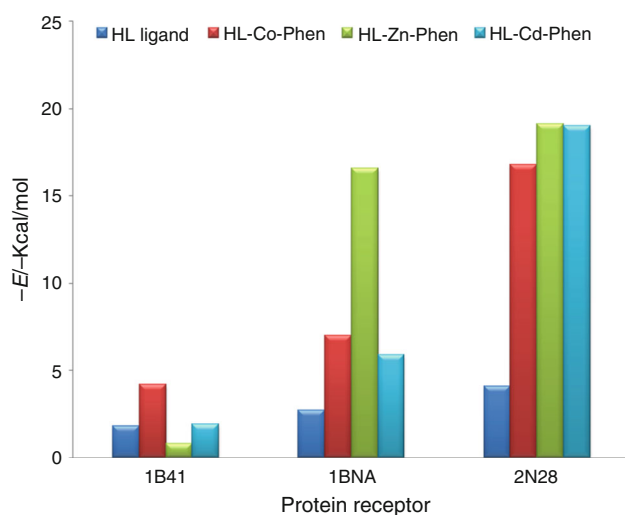


Fig. 11 Histogram of the binding energy ($-E$ kcal/mol) between ferrocene Schiff base ligand HL and its mixed ligand chelates with different protein receptors (PDB: 1B41, 1BNA and 2N28)

Conclusions

The coordination chemistry of some transition metal ions: Cr(III), Mn(II), Fe(III), Co(II), Ni(II), Cu(II), Zn(II) and Cd(II) with ferrocene-based Schiff base ligand HL (as primary ligand) and 1,10-phenanthroline (as secondary ligand) was elucidated. The metal complexes were characterized by elemental analyses, molar conductance, IR, ^1H NMR, UV-visible spectral analysis, mass spectroscopy, SEM and thermal analyses techniques. The HL ligand and its mixed ligand chelates were subjected to thermal analyses (TG and DTG). The biological activity (antimicrobial and anticancer activity) of the HL ligand and its mixed ligand complexes was also screened. Mn(II) complex showed the best IC_{50} value of $4.5 \mu\text{g mL}^{-1}$. MOE (Molecular Operating Environment) docking studies were performed using MOE 2008 software which performed docking calculations to identify the binding orientation or

conformation of prepared compounds in the active site of different proteins. The $[\text{Zn}(\text{L})(\text{Phen})(\text{Cl})(\text{H}_2\text{O})]$ complex showed the best binding ability with minimum binding energy through ionic, hydrogen acceptor and donor interactions with the tested three crystal structures (PDB) 1B41, 1BNA and 2N28.

References

- Kulkarni AK, Avaji PG, Bagihalli GB, Badami PS, Patil SA. Synthesis, spectral, electrochemical and biological studies of Co(II), Ni(II) and Cu(II) complexes with Schiff bases of 8-formyl-7-hydroxy-4-methyl coumarin. *J Coord Chem*. 2009;62:481–92.
- Nejo AA, Kolawole GA, Nejo AO. Synthesis, characterization, antibacterial, and thermal studies of unsymmetrical Schiff-base complexes of cobalt (II). *J Coord Chem*. 2010;63:4398–410.
- Mohamed GG, Omar MM, Hindy AM. Metal complexes of Schiff bases: preparation, characterization, and biological activity. *Turk J Chem*. 2006;30:361–82.
- Biyala MK, Singh RV. Structural studies with antimicrobial and antifertility activity of a monofunctional bidentate ligand with its boron(III), palladium(II), and platinum(II) complexes phosphorus. *Sulfur Silicon Relat Elem*. 2006;6:1477–91.
- Kumar D, Gupta PK, Syamal AJ. Syntheses, magnetic and spectral studies on polystyrene supported coordination compounds of bidentate and tetradentate Schiff bases. *J Chem Sci*. 2005;117:247–53.
- Britovsek GJP, Mastroianni S, Solan GA, Baugh SPD, Redshaw C, Gibson VC, White AJP, Williams DJ, Elsegood MRJ. Oligomerisation of ethylene by bis(imino)pyridyliron and -cobalt complexes. *Chem Eur J*. 2000;6:2221–31.
- Boghaei DM, Mohebi S. Synthesis, characterization and study of vanadyl tetradentate Schiff base complexes as catalyst in aerobic selective oxidation of olefins. *J Mol Catal A Chem*. 2002;179:41–51.
- Singh RV, Fahmi N, Biyala MK. Coordination behavior and biopotency of N and S/O donor ligands with their palladium(II) and platinum(II) complexes. *J Chem Soc Iran*. 2005;2:40–6.
- Elmali A, Zeyrek CT, Elerman Y, Durlu TN. Structures of four- and six-coordinate monomers of $[\text{N},\text{N}'\text{-bis}(5\text{-chlorosalicylidene})\text{-}1,3\text{-diaminopropane}]\text{nickel(II)}$. *J Chem Crystallogr*. 2000;30:167–76.
- Pal S. Copper(II) complexes with aroylhydrazones. *Proc Indian Acad Sci*. 2002;114:417–30.
- Pasini A, Bernini E, Scaglia M, Desantis G. Studies on the oxidation of CuII complexes of quadridentate Schiff bases derived from salicylaldehyde or ortho-aminophenol. *Polyhedron*. 1996;15:4461–7.
- Osoyole AA, Woods JAO, Odunola OA. Synthesis and characterization of some nickel(II) β -ketoamines and their adducts with 2,2-bipyridyl and 1,10-phenanthroline. *Synth React Inorg Metal Org Chem*. 2002;32:783–99.
- Osoyole AA, Woods JAO, Odunola OA. Synthesis and physico-chemical properties of some copper(II) β -ketoamines and their adducts with 2,2-bipyridyl and 1,10-phenanthroline. *Synth React Inorg Metal Org Chem*. 2003;33:167–82.
- Boghaei DM, Lashanizadegan M. Template synthesis and characterization of highly unsymmetrical tetradentate Schiff base complexes of Ni(II) and Cu(II). *J Sci IRI*. 2000;11:301–4.
- Boghaei DM, Sabounchei SJS, Rayti S. Synthesis and reactivity of unsymmetrical Schiff base ligand towards Ni(II), Cu(II) and Pd(II). *Synth React Inorg Metal Org Chem*. 2000;30:1535–45.
- Boghaei DM, Mohebi S. Novel unsymmetrical tetradentate Schiff base complexes of cobalt(II) and palladium(II) with N_2O_2 donor sets. *J Chem Res*. 2001;6:660–88.
- Lashanizadegan M, Boghaei DM. Template synthesis and X-ray structure determination of unsymmetrical tetradentate Schiff base complexes of nickel(II) and copper(II). *Synth React Inorg Metal Org Chem*. 2001;31:1519–29.
- Osoyole AA, Kolawole GA, Fagade OE. Synthesis, physico-chemical, and biological properties of nickel(II), copper(II), and zinc(II) complexes of an unsymmetrical tetradentate Schiff base and their adducts. *Synth React Inorg Metal Org Chem Nano-Metal Chem*. 2005;35:829–36.
- Osoyole AA. Studies of some VO(IV), Ni(II) and Cu(II) complexes on nonsymmetrical tetradentate Schiff-bases. *Chem Soc Ethiop*. 2008;22:219–24.
- El-Sonbati AZ, Diab MA, El-Bindary AA, Eldesoky AM, Morgan ShM. Correlation between ionic radii of metals and thermal decomposition of supramolecular structure of azodye complexes. *Spectrochim Acta A*. 2015;135:774–91.
- El-Ghamaz NA, Diab MA, El-Bindary AA, El-Sonbati AZ, Seyam HA. Geometrical structure and optical properties of antipyrine Schiff base derivatives. *J Mater Sci Semicond Proc*. 2014;27:521–31.
- Albert A. Selective toxicity: the physico-chemical basis of therapy. 6th ed. New York: Wiley; 1979. p. 180–234.
- Chandra S, Jain D, Sharma AK, Sharma P. Coordination modes of a Schiff base pentadentate derivative of 4-aminoantipyrine with cobalt(II), nickel(II) and copper(II) metal ions: synthesis, spectroscopic and antimicrobial studies. *Molecules*. 2009;14:174–90.
- Skehan P, Storeng R. New colorimetric cytotoxicity assay for anticancer-drug screening. *J Natl Cancer Inst*. 1990;42:1107–12.
- Abd-Elzaher MM, Labib AA, Mousa HA, Moustafa SA, Ali MM, El-Rashedy AA. Synthesis, anticancer activity and molecular docking study of Schiff base complexes containing thiazole moiety. *J Basic Appl Sci*. 2016;5:85–96.
- Dhanaraj CJ, Hassan IU, Johnson J, Joseph J, Joseyphus RS. Synthesis, spectral characterization, DNA interaction, anticancer and molecular docking studies on some transition metal complexes with bidentate ligand. *J Photochem Photobiol B Biol*. 2016;162:115–24.
- Pretsch E, Seibl J. Tables of spectral data for structure determination of organic compounds: absorption spectra of salicylaldehyde-ethylenediimine and related compounds. *Bull Chem Soc Jpn*. 1983;13:527–33.
- Emara AAA, Ali AM, El-Asmy AF, Ragab EM. Investigation of the oxygen affinity of manganese(II), cobalt(II) and nickel(II) complexes with some tetradentate Schiff bases. *J Saudi Chem Soc*. 2011;18:762–73.
- Dağlı O, Köse DA, Avcı GA, Şahin O. Novel mixed-ligand complexes of coumarilate/ N,N' -diethylnicotinamide with some transition metals. Synthesis and structural characterization. *J Therm Anal Calorim*. 2017;129(3):1389–402.
- Muhammad N, Ikram M, Rehman S, Ibrahim M, Schulzke VC. Structural, thermal kinetics and thermodynamics study of new mixed ligand zinc complexes. *J Therm Anal Calorim*. 2017;128(1):627–37.
- Mahmoud WH, Omar MM, Sayed FN. Synthesis, spectral characterization, thermal, anticancer and antimicrobial studies of bidentate azo dye metal complexes. *J Therm Anal Calorim*. 2016;124(2):1071–89.
- Soliman MH, Mohamed GG. Preparation, spectroscopic and thermal characterization of new metal complexes of verlipride drug. In vitro biological activity studies. *Spectrochim Acta A*. 2012;91:11–7.

33. Sathiyaraj S, Sampath K, Raja G, Butcher RJ, Gupta SK, Jayabalakrishnan C. DNA binding/cleavage, antioxidant and cytotoxic activities of water soluble cobalt(II) and copper(II) antipyrine complexes. *Inorg Chim Acta*. 2013;406:44–52.
34. Geary WJ. The use of conductivity measurements in organic solvents for the characterization of coordination compounds. *Coord Chem Rev*. 1971;7:81–122.
35. Refat MS, Mohamed GG, De Farias RF, Powell AK, El-Garib MS, El-Korashy SA, Hussien MA. Spectroscopic, thermal and kinetic studies of coordination compounds of Zn(II), Cd(II) and Hg(II) with norfloxacin. *J Therm Anal Calorim*. 2010;102:225–32.
36. Zayed EM, Mohamed GG, Hindy AMM. Transition metal complexes of novel Schiff base synthesis, spectroscopic characterization, and in vitro antimicrobial activity of complexes. *J Therm Anal Calorim*. 2015;120:893–903.
37. Soliman MH, Mohamed GG, Elgemeie GH. Novel synthesis of 2-imino-2H-chromene-3-carboximide metal complexes thermal decomposition, spectral studies and antimicrobial activity evaluation. *J Therm Anal Calorim*. 2016;123:583–94.
38. Mahmoud WH, Deghadi RG, Mohamed GG. Preparation, geometric structure, molecular docking thermal and spectroscopic characterization of novel Schiff base ligand and its metal chelates Screening their anticancer and antimicrobial activities. *J Therm Anal Calorim*. 2017;127(3):2149–71.
39. Thangavel S, Rajamanikandan R, Friedrich HB, Ilanchelian M, Omondi B. Binding interaction, conformational change, and molecular docking study of *N*-(pyridin-2-ylmethylene) aniline derivatives and carbazole Ru(II) complexes with human serum albumins. *Polyhedron*. 2016;107:124–35.
40. El-Ghamaz NA, El-Sonbati AZ, Diab MA, El-Bindary AA, Seyam HA. Optical properties of thermally evaporated 4-(4-nitrobenzalideneamino) antipyrine Schiff base thin films. *Solid State Sci*. 2013;19:19–26.
41. El-Ghamaz NA, Diab MA, El-Bindary AA, El-Sonbati AZ, Seyam HA. Geometrical structure and optical properties of antipyrine Schiff base derivatives. *Mater Sci Semicond Process*. 2014;27:521–31.
42. Diab MA, El-Sonbati AZ, El-Bindary AA, Morgan ShM, Abd El-Kader MK. Geometrical structures, molecular docking, spectroscopic characterization of mixed ligand and Schiff base metal complexes. *J Mol Liq*. 2016;218:571–85.
43. Tyagi P, Tyagi M, Agrawal S, Chandra S, Ojha H, Pathak M. Synthesis, characterization of 1,2,4-triazole Schiff base derived 3d-metal complexes: induces cytotoxicity in HepG2, MCF-7 cell line, BSA binding fluorescence and DFT study. *Spectrochim Acta A*. 2017;171:246–57.
44. Ilkimen H, Yenikaya C, Gülbandır A, Sarı M. Synthesis and characterization of a novel proton salt of 2-amino-6-nitrobenzothiazole with 2, 6-pyridinedicarboxylic acid and its metal complexes and their antimicrobial and antifungal activity studies. *J Mol Struct*. 2016;1120:25–33.
45. Adiguzel E, Yilmaz F, Emirik M, Ozil M. Synthesis and characterization of two new hydroxamic acids derivatives and their metal complexes An investigation on the keto/enol, E/Z and hydroxamate/hydroximate forms. *J Mol Struct*. 2017;1127:403–12.
46. Mahmoud WH, Mahmoud NF, Mohamed GG, El-Sonbati AZ, El-Bindary AA. Synthesis, spectroscopic, thermogravimetric and antimicrobial studies of mixed ligands complexes. *J Mol Struct*. 2015;1095:15–25.
47. Mahmoud WH, Deghadi RG, Mohamed GG. Spectroscopic and thermal characterization of biologically and anticancer active novel Schiff base metal complexes. *Res Chem Intermed*. 2016;42:7869–907.
48. Mahmoud WH, Mohamed GG, Mahmoud NF. New bioactive Pt(II) binary and ternary metal complexes with guaifenesin drug: Synthesis, geometrical structure, and spectroscopic and thermal characterization. *Appl Organomet Chem*. 2017;31:e3583.
49. Khan MI, Khan A, Hussain I, Khan MA, Gul S, Iqbal M, Rahman IU, Khuda F. Spectral, XRD, SEM and biological properties of new mononuclear Schiff base transition metal complexes. *Inorg Chem Commun*. 2013;35:104–9.
50. Chohan ZH, Arif M, Akhtar MA, Supuran CT. Metal-based antibacterial and antifungal agents: synthesis, characterization, and in vitro biological evaluation of Co(II), Cu(II), Ni(II), and Zn(II) complexes with amino acid-derived compounds. *Bioinorg Chem Appl*. 2006;2006:1–16.
51. Chohan ZH, Scozzafava A, Supuran CT. Complexes of benzothiazole-derived Schiff bases with antibacterial activity. *J Enzyme Inhib Med Chem*. 2003;18:259–63.
52. Yousef TA, Alduaij OK, Abu El-Reash GM, El Morshedy RM. Semiempirical studies, spectral analysis, in vitro antibacterial and DNA degradation studies of heterocyclic thiosemicarbazone ligand and its metal complexes. *J Mol Liq*. 2016;222:762–76.
53. Muhammad I, Javed I, Shahid I, Nazia I. In Vitro antibacterial studies of ciprofloxacin-imines and their complexes with Cu(II), Ni(II), Co(II), and Zn(II). *Turk J Biol*. 2007;31:67–72.
54. Thangadurai TD, Natarajan K. Ruthenium(III) complexes containing α , β -unsaturated- β -ketoaminate and their biological activities. *Indian J Chem A*. 2001;40:573–6.
55. Chohan ZH, Pervez H, Rauf A, Khan KM, Supuran CT. Isatin-derived antibacterial and antifungal compounds and their transition metal complexes. *J Enzyme Inhib Med Chem*. 2004;19:417–23.
56. Chen ZJ, Chen YN, Xu CN, Zhao SS, Cao QY, Qian SS, Qin J, Zhu HL. Synthesis, crystal structures, molecular docking, and in vitro biological activities evaluation of transition metal complexes with 4-(3,4-dichlorophenyl) piperazine-1-carboxylic acid. *J Mol Struct*. 2016;1117:293–9.
57. Alaghaz AMA, El-Sayed BA, El-Henawy AA, Ammar RAA. Synthesis, spectroscopic characterization, potentiometric studies, cytotoxic studies and molecular docking studies of DNA binding of transition metal complexes with 1,1-diaminopropane-Schiff base. *J Mol Struct*. 2013;1035:83–93.
58. Enz A, Amstutz R, Boddeke H, Gmelin G, Malanowski J. Brain selective inhibition of acetylcholinesterase: a novel approach to therapy for Alzheimer's disease. *Prog Brain Res*. 1993;98:431–8.
59. Harel M, Kryger G, Rosenberry TL, Mallender WD, Lewis T, Fletcher RJ, Guss JM, Silman I, Sussman JL. Three-dimensional structures of *Drosophila melanogaster* acetylcholinesterase and of its complexes with two potent inhibitors. *Protein Sci*. 2000;9:1063–72.
60. Kryger G, Harel M, Giles K, Toker L, Velan B, Lazar A, Kronman C, Barak D, Ariel N, Shafferman A, Silman I, Sussman JL. Structures of recombinant native and E202Q mutant human acetylcholinesterase complexed with snake-venom toxin fasciculon-II. *Acta Cryst*. 2000;56:1385–94.
61. Mahmoud WH, Mahmoud NF, GG Mohamed. Synthesis, physicochemical characterization, geometric structure and molecular docking of new biologically active ferrocene based Schiff base ligand with transition metal ions. *Appl Organomet Chem*. 2017. doi:10.1002/aoc.3858.
62. Drew HR, Wing RM, Takano T, Broka C, Tanaka S, Itakura K, Dickerson RE. Structure of a B-DNA dodecamer: conformation and dynamics. *Proc Natl Acad Sci USA*. 1981;78:2179–83.
63. Roy N, Pacini G, Berlioz-Torrent C, Janvier K. Mechanisms underlying HIV-1 Vpu-mediated viral egress. *Front Microbiol*. 2014;5:177.

64. Shah AH, Sowrirajan B, Davis ZB, Ward JP, Campbell EM, Planelles V, Barker E. Degranulation of natural killer cells following interaction with HIV-1-infected cells is hindered by downmodulation of NTB-A by Vpu. *Cell Host Microbe*. 2010;8:397–409.
65. Sowrirajan B, Barker E. The natural killer cell cytotoxic function is modulated by HIV-1 accessory proteins. *Viruses*. 2011;3:1091–111.
66. Ramirez PW, Famiglietti M, Sowrirajan B, DePaula-Silva AB, Rodesch C, Barker E, Bosque A, Planelles V. Downmodulation of CCR7 by HIV-1 Vpu results in impaired migration and chemotactic signaling within CD4(+) T cells. *Cell Rep*. 2014;7:2019–30.